Submitted as an article for *Limnology and Oceanography*

January 17, 1996

The effect of nitrogen limitation on the absorption and scattering properties of the marine diatom *Thalassiosira pseudonana*

Rick A. Reynolds, Dariusz Stramski, and Dale A. Kiefer

Department of Biological Sciences

University of Southern California

Los Angeles, CA 90089-0371 USA

Telephone: (213) 740-5813

e-mail: rick@physics1.usc.edu

Suggested running head: N-limited optical properties

Acknowledgments

This study was supported by grants from the Environmental Optics Program of the Office of Naval Research (N00014-95-1-0491), the Ocean Biogeochemistry Program of NASA (NAGW-3574), and a Department of Defense AASERT grant (N00014-93-1-0680). The carbon and nitrogen analysis was performed at the MSI analytical laboratory at the University of California, Santa Barbara.

Abstract

Optical properties of the marine diatom *Thalassiosira pseudonana* were examined in nitrate-limited semicontinuous cultures at four rates of growth. Two experiments were conducted at each growth rate in which sampling of the culture was done at either the dark-to-light (D-L) or light-to-dark (L-D) transition of a 12 h photoperiod. Optical cross-sections and efficiency factors for absorption, scattering, and attenuation were calculated from measurements of the spectral absorption and beam attenuation coefficients, cell concentration, and the size distribution of cells in suspension. The refractive index of cells was calculated from this data using an inverse method. Nitrogen limitation strongly influences the optical properties of this species. Absorption cross-sections increased more than twofold with increasing growth rate, predominantly caused by increases in the imaginary part of the refractive index, n'. Variability in n' was strongly correlated with intracellular chlorophyll *a* concentration. In contrast to absorption, scattering cross-sections were not a strong function of growth rate but exhibited significant differences between D-L and L-D experiments at any given growth rate. Variability in the real part of the refractive index was correlated with intracellular carbon concentration. The chlorophyll *a*-specific absorption coefficient decreased with increasing growth rate in response to decreases in the carotenoid to chlorophyll *a* ratio and increased pigment packaging. The chlorophyll *a*-specific scattering coefficient also decreased with increasing growth rate, and was correlated with the cellular carbon to chlorophyll *a* ratio. Our results suggest that the optical properties of phytoplankton populations in nitrogen-limited surface waters may be significantly altered from those in deeper portions of the water column.

Introduction

Advances in optical instrumentation, combined with improved modeling of radiative transfer in the ocean, allow the optical properties of seawater to be monitored over a broad range of spatial and temporal scales. For most oceanic waters, variability in the inherent optical properties of seawater can be attributed to suspended biogenic particles and associated dissolved materials. This link between the optical properties of seawater and the planktonic microbial community dictates that biological processes be included into models of radiative transfer within the ocean, and provides an opportunity to extract biological information from measurements of optical variability using appropriate inversion models.

Two of the inherent optical properties of seawater are the spectral absorption, $a(\lambda)$, and scattering, $b(\lambda)$, coefficients (see list of notation for all significant symbols and units). Phytoplankton are one constituent of the marine planktonic community which exert a strong influence on the absorption and scattering properties of seawater (e.g. Smith and Baker 1978, Morel 1988). An understanding of the optical properties of phytoplankton cells, and how they vary in the natural environment, is prerequisite to the interpretation of optical variability in the sea and to the bio-optical modeling of primary production. Variability in cellular optical properties is also of direct interest to the analysis of light scattering and fluorescence by single particles. Techniques which permit the analysis of individual cells, such as flow cytometry, are being increasingly used to study natural planktonic communities (Olson et al. 1991).

It is of particular interest to study phytoplankton growing under conditions which approximate the near surface layers of the upper ocean, as this portion of the water column contributes the dominant part of the signal viewed by instrument platforms mounted on satellites or aircraft. In large regions of the open ocean, surface waters are often characterized by relatively high levels of irradiance and low concentrations of inorganic nutrients such as nitrogen. Bio-optical relationships in this portion of the water column often deviate from those observed in the lower strata of the euphotic zone, although the causes for these changes are poorly understood (Cullen and Lewis 1995).

Cell size and refractive index are the predominant factors influencing the absorption and scattering properties of algal cells. The refractive index is closely coupled to the biochemical composition and metabolism of cell material. It is widely recognized that cell size, shape, and chemical composition of phytoplankton can change in response to the ambient conditions for growth. Although several studies have examined variability in phytoplankton biochemical composition and physiological processes in response to limitation of growth by nitrogen, only a few of these studies have provided measurements of phytoplankton optical properties (Kiefer et al. 1979, Cleveland and Perry 1987, Herzig and Falkowski 1989, Chalup and Laws 1990, Sosik and Mitchell 1991). Furthermore, with the exception of the Kiefer et al. study, these investigations have focused solely on the absorption process. To our knowledge, a detailed description of the effect of nitrogen limitation on both the absorption and scattering properties of a phytoplankton species is lacking.

The purpose of this study was to examine how limitation of growth by nitrogen influences the optical properties of the marine diatom *Thalassiosira pseudonana*. Our approach was to examine nitrogen-limited laboratory cultures at four rates of steady state growth. Measurements of the spectral absorption and beam attenuation coefficients, cell concentration, and cell size distribution in suspension were used to calculate optical cross-sections and efficiency factors at the level of a single cell. The bulk refractive index of cells was derived from this data with an inverse modeling procedure. Measurements of particulate carbon and photosynthetic pigments in suspension were used to determine how specific absorption and scattering coefficients vary in response to nitrogen limitation, and to examine relationships between cell composition and optical properties.

Materials and methods

Experimental design - The centric diatom, *Thalassiosira pseudonana* (Hustedt) Hasle et Heimdal, was obtained from the Bigelow Laboratory Culture Collection (clone 3H). This neritic species is similar in size to many eukaryotic oceanic nanophytoplankton, and is capable of

sustaining rapid growth rates in culture. Semicontinuous cultures, in which the growth rate of the population is determined by the supply of inorganic nitrogen, were grown at four rates of dilution corresponding to nitrogen-specific growth rates of 0.22, 0.51, 0.81, and 1.32 d^{-1}. Measurements were performed when the cultures had acclimated to the experimental conditions and steady state growth of the population had been established.

There is strong evidence that several characteristics of phytoplankton cells exhibit considerable variability over a diel cycle (e.g. Sournia 1974, Prézelin 1992). In a previous study with this species under nutrient replete conditions, we observed consistent increases in optical cross-sections for both absorption and scattering over the illuminated portion of the day, with minima occurring at the beginning and maxima near the end of the light period (Stramski and Reynolds 1993). To examine the potential range in optical cross-sections over a light-dark cycle in irradiance, two independent experiments were conducted at each single growth rate. In one experiment, sampling and subsequent dilution of the culture were done at the dark-to-light transition (D-L); in a second experiment, sampling and dilution were done at the light-to-dark transition (L-D).

Culturing procedures and sampling - The experimental culture vessel consisted of a water-jacketed 2-liter glass cylinder connected to a circulating water bath. A temperature of 20 °C (± 0.1 °C) within the culture was maintained for all experiments. Cells were kept in suspension by a combination of continuous stirring and bubbling with water-saturated, sterile-filtered air. Cell growth on the walls of the culture vessel was not observed in any of the experiments.

Growth irradiance was provided by fluorescent lights (Sylvania "cool white") radially located around the culture vessel. Photosynthetically available scalar irradiance (400-700 nm), measured with a quantum irradiance meter (QSL-100, Biospherical Instr.), was 345 µmol quanta m^{-2} s^{-1} at the center of the vessel and varied less than 12% throughout the culture. The cultures were maintained on a 12:12 light-dark photoperiod, yielding a daily integrated irradiance of 14.9 mol m^{-2}. This level of irradiance is similar to that commonly observed in the upper portions of the

euphotic zone (e.g. Jerlov 1976), and is sufficient to saturate growth for this species (Thompson et al. 1991).

The growth medium consisted of the artificial seawater ASPM (MacLachlan 1964) enriched, except for nitrogen, with the nutrient formulation f/2 (Guillard and Ryther 1962). Inorganic nitrogen, supplied as NO_3^-, was provided at a nominal concentration of 40 μM in the medium. Nutrient enrichments were added by sterile filtration after autoclaving of the basal medium to prevent losses or degradation. Cultures were diluted once daily with fresh media via a peristaltic pump equipped with an in-line 0.2 μm sterile filter (MediaKap-5, Microgon). Dilutions, which required approximately 1 h to complete, were done immediately after sampling to minimize the possibility of so-called "dilution effects" on measurements of cellular optical properties made on the following day (Ackleson et al. 1988). Measurements of inorganic nutrient concentrations in samples removed from the vessel confirmed that nitrogen was depleted in the culture (< 1 μM) after a 24 h period.

The beam attenuation coefficient of the culture (described below) was monitored daily before dilution, and cultures were considered to be in steady state when this parameter varied by less than 5% over a period of 7 to 12 days. At this time measurements began and were repeated on the culture over a period of 3 to 4 successive days. The data obtained from each individual day were analyzed independently and subsequently averaged over all days; unless noted otherwise our results are reported as the mean value obtained for each experiment with the coefficient of variation (C.V. = SD/mean) in percent describing the reproducibility among individual days.

As a precaution, all samples used in optical and biological measurements were prefiltered with 10 μm Nitex mesh to remove aggregates. Microscopic examination of non-prefiltered samples indicated that cells present in aggregates comprised a small percentage of the total cell population in each experiment (< 5%).

Cell enumeration, growth rates, and size distributions - To determine cell concentration (number per unit volume) in the cultures, 9-ml subsamples were preserved with 0.2 μm filtered

formaldehyde buffered in seawater (0.2% v/v final concentration) and stored in the dark at 4 °C. All samples were analyzed within 2 weeks of the experiment. Cell concentration was determined by microscopic counts (100x magnification) in a Bright-Line hematocytometer with improved Neubauer ruling (Reichert). A minimum of 3000 cells were counted for each individual sample, the precision of these measurements was usually better than 12%.

Additional samples which were not prefiltered with Nitex were taken at both the time of sampling and immediately after dilution with fresh media to estimate rates of population growth from daily changes in culture biomass. Because nitrogen was assumed to be limiting, daily changes in particulate nitrogen were chosen as the most appropriate measure of population growth. Nitrogen-specific growth rates were calculated as

$$\mu_N = \frac{1}{\Delta t} \ln(N_t/N_0) \qquad (1)$$

where N_0 is the concentration of particulate nitrogen in the culture after dilution and N_t is the concentration at the time of sampling on the following day (before dilution). N_0 was calculated using the cell concentration measured after dilution and the nitrogen content per cell measured immediately before dilution. Similar estimates of specific growth rates were also calculated for other measures of biomass such as particulate carbon and chlorophyll *a*.

The size distribution of cells in suspension was measured at the time of sampling with a Coulter counter model ZBI equipped with a 50 µm orifice and coupled to a C-1000 Channelyzer. The instrument was calibrated with both 3 and 5 µm latex microspheres (Coulter Instr.), with filtered media (0.22 µm, filtered 5x) used as the diluent and as the blank. Replicate measurements of the cell size distribution were made on each sample at two instrument sensitivities and the results combined to yield the relative size distribution. A minimum of 10^5 cells were sized for each sample.

No attempt was made to directly determine cell concentration with the Coulter counter, instead the relative number of cells in each size class was scaled so that the integrated count was

equal to the concentration of cells determined from microscopic counts. The resulting size distribution, F(D) dD, represents the number of cells per unit volume with equivalent spherical diameter between D and D+dD. In all calculations we thus assume that the cells are spherical in shape, a reasonable approximation for this species. The volume of a "mean" cell, $\overline{V}$, characterizing the population was derived by integration of the size distribution between the minimum and maximum diameter of the population (D_{min} and D_{max}, respectively).

$$\overline{V} = \frac{\pi}{6} \int_{D_{min}}^{D_{max}} D^3 F(D) dD \left[\int_{D_{min}}^{D_{max}} F(D) dD \right]^{-1} \quad (2)$$

The geometrical projected area of a mean cell, $\overline{G}$, and the corresponding mean diameter, $\overline{D}$, were also calculated (see Eqs. 1 and 2 of Stramski and Reynolds 1993).

Photosynthetic pigments, carbon, and nitrogen determinations - Duplicate samples for the determination of photosynthetic pigments were filtered onto glass fiber filters (Whatman GF/F), homogenized in 90% acetone with a teflon tissue grinder, and extracted 24 h at 4 °C. The extracts were clarified by centrifugation and the concentrations of chlorophylls *a* and *c* determined spectrophotometrically using the equations of Jeffrey and Humphrey (1975). Concentrations of total carotenoid pigments were estimated from the extracts following the procedure described in Parsons et al. (1984).

Samples for particulate organic carbon, C, and nitrogen, N, were filtered onto precombusted GF/F filters, flash frozen in liquid nitrogen, and stored at -80 °C until analysis. C and N content of the filters was measured by a standard dry combustion technique with a Leeman Labs model CE 440 analyzer.

Cell quotas for carbon, nitrogen, and pigmentation were calculated by normalizing the respective concentration in suspension to the cell concentration. Intracellular concentrations of carbon, C_i, and chlorophyll *a* , Chl a_i, were determined by dividing the mean cell quotas by the

mean cell volume. Emphasis is placed on intracellular concentrations as they are the most appropriate to the interpretation of cell optical properties.

Measurement of optical properties - The general procedures for our optical measurements are described in Stramski and Reynolds (1993) and are briefly reviewed here. The spectral absorption, $a(\lambda)$, and beam attenuation, $c(\lambda)$, coefficients of the culture were measured in 1-cm quartz cuvettes with a dual beam spectrophotometer (Uvikon 860, Kontron). Measurements were made in the spectral region 350 to 750 nm at 1-nm resolution, with filtered media from the culture (0.2 μm syringe filter, Nalgene) used to determine instrument baseline and as the reference. The suspensions were optically thin which ensured that multiple photon-particle interactions were negligible (e.g. Morel and Bricaud 1986). Triplicate scans were obtained for each sample and corrected for baseline. Individual scans were smoothed twice with a 5-nm moving average, and then averaged to produce the final spectrum. Reproducibility of the three scans at visible light wavelengths was better than 4% for both $a(\lambda)$ and $c(\lambda)$.

Absorption was measured by placing the cuvettes at the entrance to an integrating sphere with an effective half-angle of acceptance of ~45°. To correct for scattering losses, we assumed that this species exhibits no absorption at 750 nm (see Stramski and Reynolds 1993), and spectra were adjusted accordingly with a λ-independent correction. In contrast to absorption, beam attenuation measurements were made with a modified geometric configuration of the instrument which reduced the acceptance angle of the detector to <1°. The spectral scattering coefficient, $b(\lambda)$, was calculated as the difference between $c(\lambda)$ and $a(\lambda)$.

Computation of optical cross-sections, efficiency factors, and refractive index - In general, the optical properties of a seawater suspension result from the sum of the contributions by the individual constituents present in the suspension. These constituents include the seawater itself, dissolved substances, and particulate material which includes living as well as non-living particles. In the present experiment, filtered media from the culture was used as the reference

and the cultures were visually free of detritus, thus we attribute the measured optical signal entirely to the algal cells present in the suspension.

The experimental data were used to calculate the optical properties of *T. pseudonana* at the level of a single cell. Optical cross-sections for absorption, $\overline{\sigma}_a(\lambda)$, scattering, $\overline{\sigma}_b(\lambda)$, and attenuation, $\overline{\sigma}_c(\lambda)$, were calculated by normalizing the respective bulk optical coefficient (a, b, or c) to the cell concentration. Some variability in optical cross-sections between individual algal cells is expected, and thus the bar above the symbol indicates that this quantity represents a hypothetical "mean" cell derived from the actual polydispersed population. The dimensionless efficiency factors for absorption, $\overline{Q}_a(\lambda)$, scattering, $\overline{Q}_b(\lambda)$, and attenuation, $\overline{Q}_c(\lambda)$, of the mean cell were calculated as the ratio of the respective optical cross-section to the cell projected area $\overline{G}$.

The optical efficiency factors (and thus the cross-sections) depend upon both the cell size and complex index of refraction, $m(\lambda) = n(\lambda) - i\,n'(\lambda)$, where n and n' represent the relative real and imaginary parts respectively. Utilizing an inverse method, the experimental measurements of cell size distribution and optical efficiency factors were used to calculate the refractive index of the cells relative to seawater. In this calculation, the theoretical estimates of $\overline{Q}_a(\lambda)$ and $\overline{Q}_c(\lambda)$ are varied iteratively at each wavelength λ as a function of a single variable, n' and n respectively, until these estimates match their experimental counterparts (Bricaud and Morel 1986, Stramski et al. 1988). The theoretical formulation for Q_a (Duysens 1956, van de Hulst 1957) and Mie calculations for Q_c (Bohren and Huffman 1983) representing homogeneous spherical particles were used. Values for n' were derived first, and were included as additional inputs to the Mie calculations for determining n.

Chlorophyll *a*- and carbon-specific optical coefficients were calculated by normalizing $a(\lambda)$, $b(\lambda)$, and $c(\lambda)$ to the concentrations of Chl a and C within the suspension.

Results

Biomass, growth rates, and cell size - Cell concentration in the cultures at steady state decreased twofold with increasing rates of growth, although total particulate nitrogen was independent of growth rate (not shown). Specific growth rates determined from daily changes in particulate nitrogen (μ_N, Eq. 1) varied from 0.22 to 1.32 d^{-1} (Table 1), and were identical to rates predicted from dilution with fresh media. Similar results were obtained for growth rates calculated from changes in C and Chl a within the culture. Steady state growth could not be maintained for growth rates exceeding 1.32 d^{-1}.

Fig. 1 illustrates changes in the cell size distribution with growth rate. The largest mean cell size was observed at the fastest μ_N, but no apparent trend was observed over the range of slower growth rates. The mean cell volume based on all eight experiments was 63 μm^3, and varied ±15% from this value (Table 1). Most of this variation was associated with differences between D-L and L-D experiments at a single growth rate; mean cell size was larger in the L-D transition experiments with the exception of the fastest μ_N. This increase was accompanied by an increase in the modal diameter of the population, as well as a tendency for the size distributions to be broader at this time. The cell projected area $\overline{G}$ averaged 18.7 μm^2 for all experiments and ranged from 17.0 to 20.5 μm^2.

Cell composition and pigmentation - Changes in mean cell elemental composition and pigmentation with growth rate are listed in Table 1. Because changes in cell volume were small over the range of growth rates, normalization of cellular constituents (e.g. carbon, chlorophyll *a*) to cell volume yields similar trends as normalization to cell concentration. Intracellular carbon concentration C_i in all L-D transition experiments averaged 189 kg m^{-3} (C.V.=2.1%) and varied little with growth rate. In contrast, C_i in the D-L transition experiments decreased regularly with increasing μ_N. As a result, the range in C_i between experiments at a given growth rate increased with increasing growth rate.

The ratio of cellular carbon to nitrogen, C:N, increased with nitrogen limitation (Table 1), consistent with previous studies of this species (Caperon and Meyer 1972, Eppley and Renger 1974) and with studies of other phytoplankton taxa (e.g. Herzig and Falkowski 1989, Chalup and Laws 1990, Sosik and Mitchell 1991). With the exception of the slowest μ_N, C:N ratios were significantly higher in the L-D transition experiments. This divergence between the D-L and L-D transition experiments increased with increasing μ_N; at the fastest growth rate C:N was 2.7-fold higher in the L-D experiment than in the D-L experiment. This pattern is consistent with the diel trend observed in nutrient replete *T. pseudonana* by Stramski and Reynolds (1993), in which C:N values systematically increased over the illuminated portion of day. Measured values of C:N in the present study approached the Redfield ratio only at the fastest growth rate in the D-L transition experiment.

Intracellular concentrations of chlorophyll *a*, Chl a$_i$, and carotenoids, Car$_i$, both increased with growth rate (Table 1), a common feature of nitrogen-limited growth in phytoplankton. Chl a$_i$ increased by 209% over the range of μ_N studied, with no significant difference observed between D-L and L-D experiments. The corresponding increase in carotenoid pigments with growth rate was smaller relative to increases in Chl a, resulting in a 50% decrease in the Car:Chl a ratio. Car:Chl a ratios were consistently higher in the L-D transition experiments. In contrast to the Car:Chl a ratio, variations in the chlorophyll *c*: *a* ratio with growth rate were small (data not shown).

The ratio of cell carbon to chlorophyll *a*, C:Chl a, was strongly correlated with growth rate. Mean values for the C:Chl a ratio ranged from 28 to 170 g/g, with the highest values corresponding to the slowest growing cells. At a single μ_N , C:Chl a ratios were always higher for experiments in which sampling occurred at the L-D transition.

Refractive index - The imaginary part of the refractive index, $n'(\lambda)$, increased systematically with increasing μ_N with no significant difference between the D-L and L-D transition experiments (Fig. 2A). This figure illustrates changes in n' for the blue (λ=436 nm) and red

(λ=673 nm) absorption bands of Chl a *in vivo*. The largest increases occurred within the red absorption band, where n' increased more than twofold over the range of μ_N studied. Similar trends in n' were observed in other portions of the visible spectrum, including regions of weak absorption.

The real part of the refractive index, $n(\lambda)$, as a function of growth rate is shown in Fig. 2B. We have chosen to present data for λ=660 nm, as this spectral region is routinely used to measure beam attenuation in the ocean. Values for $n(660)$ varied from 1.024 to 1.039, within the range of commonly reported values for marine diatoms (Bricaud et al. 1988). For L-D transition experiments, $n(660)$ was independent of μ_N and averaged 1.037 (C.V. = 0.1%). Values for $n(660)$ were consistently lower for the D-L transition experiments, and decreased systematically with increasing growth rate. Because of this behavior, larger variability in n between experiments is observed with increasing μ_N. At the fastest μ_N , the refractive increment (n-1) for the D-L experiment was 35% lower than in the L-D experiment.

Absorption and scattering cross-sections - Both the magnitude and spectral shape of absorption cross-sections were strongly influenced by nitrogen limitation. Spectral absorption curves exhibited peaks characteristic of chlorophylls *a* and *c* and carotenoids (Fig. 3A). Slowly growing cells exhibited the smallest values for $\bar{\sigma}_a(\lambda)$, with values increasing regularly with increasing μ_N (Fig. 3B). In the red absorption band of Chl a, $\bar{\sigma}_a$ increased 2.7-fold with increasing growth rate. Increases in blue absorption with growth rate were smaller, resulting in a 26% decrease in the blue to red absorption ratio. With the exception of the fastest growth rate, $\bar{\sigma}_a$ values were larger in the L-D transition experiments .

The shape of spectral scattering was weakly λ-dependent for the D-L transition experiments (Fig. 4A), and exhibited broad maxima in the spectral bands corresponding to weak absorption (~550 nm). In contrast, $\bar{\sigma}_b(\lambda)$ in L-D transition experiments displayed a positive slope with increasing wavelength, with maxima shifted towards the red spectral region. In addition to these general patterns, scattering cross-sections had major spectral features associated with the

absorption bands of Chl a which became more pronounced at faster growth rates (i.e. higher Chl a_i)

The observed changes in the spectral shape of scattering lead to a λ-dependence in the relationship between $\overline{\sigma}_b$ and growth rate. Large variability in $\overline{\sigma}_b$ between experiments is observed in the green to red spectral region, this variability is reduced towards shorter light wavelengths. For the L-D transition experiments, $\overline{\sigma}_b$ (660) was weakly dependent on μ_N (Fig. 4B), and this pattern was similar for all λ>550 nm. In the blue spectral region, however, $\overline{\sigma}_b$ decreased approximately 15% with increases in growth rate. In contrast to the L-D experiments, $\overline{\sigma}_b(\lambda)$ for the D-L transition experiments declined with increasing μ_N at all visible light wavelengths, with the largest decreases occurring in the red spectral region (Fig. 4B).

As in most algal cells, scattering dominates the attenuation process in *T. pseudonana*. Scattering-to-absorption ratios (b:a) were strongly influenced by growth rate, increasing more than twofold with decreases in μ_N. The largest variability occurred within the red (673 nm) absorption bands of Chl a, where the average b:a ratio increased threefold over the range of growth rates (Fig. 5). This trend was observed consistently in all other light wavelengths, including spectral areas of weak absorption (e.g. λ=550 nm).

Specific optical properties - In contrast to $\overline{\sigma}_a$, absorption coefficients normalized to Chl a, a^*_{Chl}, declined with increasing growth rate with only small differences observed between experiments at a single μ_N (Fig. 6A). In the blue absorption band of Chl a, the average a^*_{Chl} obtained for $\mu_N = 0.22\ d^{-1}$ was 0.045 m^2 (mg Chl a)$^{-1}$ and decreased by 43% with increasing growth rate. In the red absorption band of Chl a, a^*_{Chl} averaged 0.0204 m^2 (mg Chl a)$^{-1}$ for μ_N = 0.22 d^{-1} and decreased by 23% with increasing growth rate.

Chl a-specific scattering, b^*_{Chl}, was also strongly influenced by growth rate (Fig. 6B). For most light wavelengths, b^*_{Chl} was larger in the L-D transition experiments. At λ=660, b^*_{Chl} increased more than threefold with decreases in growth rate. This pattern was essentially

identical for all wavelengths. Similar results were observed for Chl a-specific attenuation (not shown).

In the previous study of *T. pseudonana* we observed that diel changes in carbon-specific attenuation were considerably smaller than changes in cross-sections on a per cell basis (Stramski and Reynolds 1993). The measurements in the present study suggest that carbon-specific attenuation (and scattering) is also independent of nitrogen-limited growth rate with this species. The average value obtained for the C-specific attenuation coefficent (λ=660 nm) in the present experiments was 3.47 m^2 $(g\ C)^{-1}$ with small variations about this value (C.V. = 4.7%), which agrees to within 10% of the mean value reported in our earlier study.

Discussion

We are confident that our results reflect changes in cellular composition and optical properties in response to limitation of growth by nitrogen. The biological responses to nitrogen limitation observed in our experiments are consistent with previous studies of this species (Caperon and Meyer 1972, Eppley and Renger 1974), and measured specific growth rates (based on N, C, and Chl a) were identical to those predicted from dilution. No significant differences were observed in these rates between D-L and L-D transition experiments, indicating that the time of dilution had no effect on the net specific growth rates of the cultures.

The patterns observed between D-L and L-D transition experiments at a single growth rate are generally consistent with the previous study of diel variability in this species (Stramski and Reynolds 1993). However, because of our experimental design we caution against a simple interpretation of these features solely as responses to a diel cycle in irradiance. The variability observed between experiments at a single growth rate is potentially influenced by several features of phytoplankton growth; these include true diel patterns initiated by a day-night cycle, circadian rhythms driven by biological clocks, or the point in the population growth cycle at which measurements are made. Some variability may also result from physiological responses to dilution at different portions of the photoperiod. We consider it likely that some portion of the

variability observed between D-L and L-D experiments (within a given growth rate) reflects differences in the point of the cell division cycle in which measurements were made. Without more detailed temporal information on population division rates, we can only interpret differences in experiments at a single growth rate as a potential range in the measured characteristics; actual diel variability may be greater or smaller than observed with our experimental design.

Variability in optical cross-sections with nitrogen limitation - Our results clearly indicate that absorption cross-sections are strongly influenced by nitrogen limitation of growth. We observed greater than twofold decreases in $\overline{\sigma}_a(\lambda)$ with decreasing μ_N, consistent with the common perception that nitrogen limitation limits the light harvesting capability of algal cells. Variability in the optical cross-sections can be interpreted in regards to changes in both cell size and refractive index through the general relationship

$$\overline{\sigma}_j(\lambda) = \overline{G}\ \overline{Q}_j(\lambda) \tag{3}$$

in which j is introduced to represent either a, b, or c. The effect of cell size on $\overline{\sigma}_j$ is twofold; directly through $\overline{G}$ and indirectly through the efficiency factor $\overline{Q}_j$. $\overline{Q}_j$ is further influenced by changes in the refractive index (specifically the imaginary part in the case of absorption efficiency). Using an analysis similar to that outlined in Stramski et al. (1995), we assessed the relative importance of changes in cell size and the imaginary part of the refractive index, n', to the observed changes in $\overline{\sigma}_a$ over the range of growth rates. For example, as μ_N increased from 0.22 to 1.32 d^{-1} we observed a 172% increase in $\overline{\sigma}_a(673)$. The results of our calculations suggest that variability in n' was the primary factor contributing to this increase, sufficient to explain 75% of the observed increase in $\overline{\sigma}_a$. The remaining 25% of this increase could be attributed to increased cell size, both directly through $\overline{G}$ and indirectly through $\overline{Q}_a$. However, changes in cell size were more important in contributing to variability between D-L and L-D

experiments at a given growth rate, as differences in n' between experiments at a single μ_N were small.

In contrast to absorption, our results suggest that scattering cross-sections are not a strong function of nitrogen-limited growth rate for this species. However, at any given μ_N there was a significant difference in $\bar{\sigma}_b(\lambda)$ between D-L and L-D experiments, with the highest variability occurring in the green to red portions of the spectrum. The observed changes in the spectral shape of scattering are explained by the general oscillatory pattern of the $\bar{Q}_b$ vs. $\bar{\rho}$ relationship, where $\bar{\rho} = 2\pi\bar{D}n_w(n\text{-}1)/\lambda$ (n_w is the refractive index of seawater, assumed to be a real number). The behavior of this function is described in detail elsewhere (van de Hulst 1956). The range of $\bar{\rho}$ calculated for this species indicate that values of $\bar{Q}_b$ are near the first maximum of this theoretical curve. The combination of higher values for $\bar{D}$ and $n(\lambda)$ in the L-D transition experiments result in $\bar{\rho}$ values such that most of the spectrum resides on the descending slope (past the first maximum) of the $\bar{Q}_b(\bar{\rho})$ function; thus $\bar{Q}_b$ (and $\bar{\sigma}_b$) increases with λ throughout most of the spectrum. In contrast, lower values for $\bar{\rho}$ in the D-L transition experiments result in a maximum $\bar{Q}_b$ near λ=550 nm, with $\bar{Q}_b$ then declining with λ at longer wavelengths.

Variability in the refractive index - Our results imply that variability in the refractive index contributes significantly to changes in the optical cross-sections of this species. The refractive index of phytoplankton cells is predominantly governed by the intracellular concentrations of organic materials and water (Aas 1981), thus variability in the refractive index arises from changes in cellular biochemical composition and metabolism resulting from acclimation to ambient environmental conditions. Because of the large range in cellular composition observed in this study, it is of interest to examine the relationships between the refractive index and major biochemical constituents of the cell.

The imaginary part of the refractive index, n', is proportional to the absorption coefficient of cellular material and thus strongly dependent upon cellular pigmentation. In the red absorption band of Chl a the contribution of other pigments to absorption is negligible, and $n'(673)$ can be

directly related to Chl a_i (Stramski and Reynolds 1993, Stramski et al. 1995). A strong linear correlation between $n'(673)$ and the intracellular concentration of Chl a was observed in this study (Fig. 7A). The intercept of this relationship is close to zero, verifying that cellular compounds other than Chl a have little influence on absorption in this spectral region. The slope parameter indicates that $n'(673)$ increases, on average, 0.00065 in response to a 1 kg m^{-3} rise in the intracellular concentration of Chl a. This value is 23% lower than that obtained in a similar calculation by Stramski and Reynolds (1993) for the same species under nutrient replete conditions. This difference may result, in part, from the large scatter in data evident in the previous study, as well as some methodological differences between the two studies.

The real part of the refractive index is dependent primarily upon the cell volume occupied by solid materials and water. Diatoms often have a large proportion of cell volume occupied by vacuoles (Werner 1977), which may explain the low values of refractive index observed in this study and others (Bricaud et al. 1988). Because carbon is a principle component of most cellular solid materials, a high degree of correlation between n and intracellular carbon concentration is expected (e.g. Stramski and Morel 1990, Morel and Ahn 1990). In the present experiments, a strong linear relationship exists between $n(660)$ and C_i over a twofold range in C_i (Fig. 7B). We note that the variability in C_i observed in this study arises principally from differences between D-L and L-D experiments; the highest values of C_i (>160 kg m^{-3}) represent mostly L-D transition experiments and are independent of growth rate. The smaller values of C_i represent D-L transition experiments, in which C_i decreases with increasing growth rate. The slope parameter of the relationship presented in Fig. 7B, $1.3 \cdot 10^{-4}$ m^3 $(kg\ C)^{-1}$, represents the average C-specific increment of the refractive index over the entire range of C_i.

By assuming average concentrations of organic compounds and water in heterotrophic bacteria, Morel and Ahn (1990) calculated a value of $2.33 \cdot 10^{-4}$ m^3 $(kg\ C)^{-1}$ for the C-specific increment of the refractive index. This value has been suggested to be applicable to several types of microbial cells, including cyanobacteria and heterotrophic flagellates (Morel and Ahn 1991). The results of this study and others (Stramski and Morel 1990, Stramski and Reynolds 1993,

Stramski et al. 1995) suggest, however, that significant variations in the C-specific increment are generally possible for various species grown under different laboratory conditions, with values ranging from 1.3 to $2.4 \cdot 10^{-4}$ m^3 $(kg\ C)^{-1}$.

Specific optical properties - It is often useful to normalize the biological and optical properties of phytoplankton to pigment content. Chl a-specific absorption, for example, is frequently used in studies of phytoplankton growth and primary production, as well as in algorithms for retrieving pigment concentrations from remotely-sensed spectral reflectance. It is recognized that such specific optical coefficients can vary considerably with the physiological status of algal cells, and thus are influenced by the ambient conditions for growth.

Our results indicate that nitrogen limitation leads to increases in the Chl a-specific absorption coefficient in this species. Variability in a^*_{Chl} can result from the effects of "pigment packaging" (Duysens 1956, Morel and Bricaud 1981), from changes in the abundance of accessory light harvesting pigments relative to Chl a (Berner et al. 1989), or both. Our data suggest that both phenomena contribute to variability in a^*_{Chl} in response to nitrogen limitation. We observed significant increases in the Car:Chl a with decreasing growth rate, this increases apparent Chl a-specific absorption in the spectral absorption bands of carotenoid pigments (primarily in the blue to green regions). In addition to such compositional changes, the large reduction in cellular pigmentation as cells become increasingly nitrogen-limited leads to increases in a^*_{Chl} as the package effect is reduced.

Our data agree with models of pigment packaging (e.g. Morel and Bricaud 1981) which predict an inverse relationship between a^*_{Chl} and the product Chl a_i $\overline{D}$ (Fig. 8A). The largest variability in a^*_{Chl} is observed in the spectral regions where $\lambda<600$ nm, reflecting the combined effects of changes in pigment composition and pigment packaging. At $\lambda=673$ nm, the contribution to absorption by pigments other than Chl a can be neglected and thus changes in $a^*_{Chl}(673)$ can be interpreted solely in regards to pigment packaging. The average value of $a^*_{Chl}(673)$ observed at the slowest growth rate, 0.0204 m^2 $(mg\ Chl\ a)^{-1}$, is not statistically

different from the commonly accepted specific absorption coefficient of 0.0202 m^2 (mg Chl a)$^{-1}$ for Chl a dissolved in 90% acetone at λ=664 nm (Jeffrey and Humphrey 1975). If one assumes that this value represents the maximum a^*_{Chl} *in vivo*, then the most nitrogen-limited cells in our study are essentially free from the effects of pigment packaging. Our data indicate that over a sixfold range of nitrogen-limited growth rates for this species, pigment packaging leads to a 23% decrease in $a^*_{Chl}(673)$. Similar results have also been reported for the marine chlorophyte *Dunaliella tertiolecta* (Sosik and Mitchell 1991).

The Chl a-specific scattering coefficient, $b^*_{Chl}(\lambda)$, varied markedly with growth rate. Our data indicate that variations in b^*_{Chl} result principally from the normalization of scattering to varying cellular Chl a content, and not from changes in the magnitude of cell scattering *per se*. It has been previously observed that the scattering coefficient of a phytoplankton suspension is related to the carbon concentration (Stramski and Morel 1990). In such cases, variability in b^*_{Chl} should be correlated with the cellular C:Chl a ratio. A very high correlation for this relationship was observed in the present experiments (Fig. 9). The intercept is not significantly different from zero, predicting the absence of scattering without the presence of cellular carbon (solid material). The slope parameter, 3.2 m^2 $(gC)^{-1}$, represents the average C-specific scattering coefficient. The strong relationship evident here supports our previous results (Stramski and Reynolds 1993) that a constant value of carbon-specific scattering (and attenuation) can be reasonably assumed for this species.

Relevance to field studies - Although laboratory studies on single species are not easily extrapolated to explain field measurements, some generalizations can be inferred. Oligotrophic waters are often characterized by the predominance of small phytoplankton species (Chisolm 1992). For such species the optical efficiency factors, and thus the optical cross-sections, are very sensitive to changes in cell size and refractive index.

Large variability in phytoplankton C_i over a light-dark cycle is expected because of photosynthetic accumulation of carbon during the light period and respiratory losses of carbon at

night. Both photosynthetic rates and respiratory rates generally increase at faster growth rates (Geider 1992). Therefore, one might anticipate a larger diel signal in the real part of the refractive index and scattering cross-sections in rapidly growing populations.

Decreases in intracellular pigmentation, accompanied by increases in Car:Chl a and C:Chl a ratios, appear to be general responses of phytoplankton to limitation of growth by nutrients such as nitrogen. Qualitatively, this response to nutrient limitation resembles acclimation to high growth irradiance. In oligotrophic surface waters, the combination of high irradiance and low nutrient concentrations are likely to reinforce one another. In such cases, one might expect distinct differences between phytoplankton optical properties at the surface and the underlying waters of the euphotic zone. This should be considered when extrapolating optical measurements from nutrient poor well-illuminated surface layers throughout the water column.

Our results suggest that phytoplankton cells in nitrogen-limited waters will be characterized by relatively low values for the imaginary part of the refractive index and small absorption cross-sections, near maximal values for Chl a-specific absorption, and high scattering-to-absorption ratios. Changes in the Car:Chl a ratio with nitrogen limitation alter the spectral shape of absorption (increase of the blue to red absorption ratio), which may hinder efforts to derive pigment concentrations of surface waters from a single standard absorption curve for phytoplankton. In addition, high b:a ratios may also have implications for remote sensing algorithms. If one can assume that b covaries with backscattering, then nutrient-limited phytoplankton cells may have an increased backscattering to absorption ratio as compared to cells growing in nutrient rich waters.

Historically, variability in the optical properties of seawater associated with particles has been interpreted as resulting from changes in particle concentration, assuming that the optical properties of the particles themselves remain constant. It is clear, however, that physiological responses to ambient growth conditions may lead to large variability in the optical properties of microorganism cells. Such variability should be recognized in future models of oceanic optics and primary production.

References

Aas, E. 1981. The refractive index of phytoplankton. Univ. Oslo Inst. Rep. Ser. 46. 61 p.

Ackleson, S. G., R. W. Spinrad, C. M. Yentsch, J. Brown, and W. Korjeff-Bellows. 1988. Phytoplankton optical properties: Flow cytometric examinations of dilution-induced effects. Appl. Opt. **27**: 1262-1269.

Berner, T., Z. Dubinsky, K. Wyman, and P. G. Falkowski. 1989. Photoadaptation and the "package" effect in *Dunaliella tertiolecta* (Chlorophyceae). J. Phycol. **25**: 70-78.

Bohren, C. F., and D.R. Huffman. 1983. Absorption and scattering of light by small particles. Wiley.

Bricaud, A., A. Bedhomme, and A. Morel. 1988. Optical properties of diverse phytoplanktonic species: experimental results and theoretical interpretation. J. Plankton Res. **10**: 851-873.

Bricaud, A., and A. Morel. 1986. Light attenuation and scattering by phytoplanktonic cells: A theoretical modeling. Appl. Opt. **25**: 571-580.

Caperon, J. and J. Meyer. 1972. Nitrogen-limited growth of marine phytoplankton- I. Changes in population characteristics with steady-state growth rate. Deep-Sea Res. **19**: 601-618.

Chalup, M. A. and E. A. Laws. 1990. A test of the assumptions and predictions of recent microalgal growth models with the marine phytoplankter *Pavlova lutheri*. Limnol. Oceanogr. **35**: 583-596.

Chisolm, S. W. 1992. Phytoplankton size, p. 213-237. *In* P.G. Falkowski and A.D. Woodhead [eds.], Primary Productivity and Biogeochemical Cycles in the Sea. Plenum Press.

Cleveland, J. S. and M. J. Perry. 1987. Quantum yield, relative specific absorption and fluorescence in nitrogen-limited *Chaetoceros gracilis*. Mar. Biol. **94**: 489-497.

Cullen, J. J., and M. R. Lewis. 1995. Biological processes and optical measurements near the sea-surface: Some issues relevant to remote sensing. J. Geophys. Res. **100**: 13255-13266.

Duysens, L. M. 1956. The flattening of the absorption spectra of suspensions as compared to that of solutions. Biochim. Biophys. Acta **19**: 1-12.

Eppley, R. W. and E. H. Renger. 1974. Nitrogen assimilation of an oceanic diatom in nitrogen-limited continuous culture. J. Phycol. **10**: 15-23.

Geider, R. J. 1992. Respiration: Taxation without representation?, p. 333-360. *In* P.G. Falkowski and A.D. Woodhead [eds.], Primary Productivity and Biogeochemical Cycles in the Sea. Plenum Press.

Guillard, R. R. L., and J. H. Ryther. 1962. Studies of marine planktonic diatoms. 1. *Cyclotella nana* Hustedt and *Detonula confervacea* (Cleve) Gran. Can. J. Microbiol. **8**: 229-239.

Herzig, R. and P. G. Falkowski. 1989. Nitrogen limitation in *Isochrysis galbana* (Haptophyceae). I. Photosynthetic energy conversion and growth efficiency. J. Phycol. **25**: 462-471.

Jeffrey, S. W., and G. F. Humphrey. 1975. New spectrophotometric equations for chlorophylls *a*, *b*, c_1, and c_2 in higher plants, algae and natural phytoplankton. Biochem. Physiol. Pflanz. **167**: 374-384.

Jerlov, N. G. 1976. Marine optics. Elsevier.

Kiefer, D.A., R. J. Olson, and W H. Wilson. 1979. Reflectance spectroscopy of marine phytoplankton. Part 1. Optical properties as related to age and growth rate. Limnol. Oceanogr. **24**: 664-672.

MacLachlan, J. 1964. Some considerations of the growth of marine algae in artificial media. Can. J. Microbiol. **10**: 769-782.

Morel, A. 1988. Optical modeling of the upper ocean in relation to its biogenous matter content (case I waters). J. Geophys. Res. **93**: 10749-10768.

Morel, A. 1991. Optics of marine particles and marine optics, p. 141-188. *In* S. Demers [ed.], Particle Analysis in Oceanography. NATO ASI Series G27, Springer-Verlag.

Morel, A., and Y. H. Ahn. 1990. Optical efficiency factors of free-living marine bacteria: Influence of bacterioplankton upon the optical properties and particulate organic carbon in oceanic waters. J. Mar. Res. **48**: 145-175.

Morel, A., and Y. H. Ahn. 1991. Optics of heterotrophic nanoflagellates and ciliates: A tentative assessment of their scattering role in oceanic waters compared to those of bacterial and algal cells. J. Mar. Res. **49**: 177-202.

Morel, A, and A. Bricaud. 1981. Theoretical results concerning light absorption in a discrete medium, and application to specific absorption of phytoplankton. Deep Sea Res. **28**: 1375-1393.

Morel, A, and A. Bricaud. 1986. Inherent optical properties of algal cells including picoplankton: Theoretical and experimental results., p. 521-555. *In* Photosynthetic picoplankton. Can. Bull. Fish. Aquat. Sci. 214.

Olson, R. J., E. R. Zettler, S. W. Chisolm, and J. Dusenberry. 1991. Advances in oceanography through flow cytometry, p. 351-399. *In* S. Demers [ed.], Particle Analysis in Oceanography. NATO ASI Series G27, Springer-Verlag.

Parsons, T. R., Y. Maita, and C. M. Lalli. 1984. A manual of chemical and biological methods for seawater analysis. Pergamon Press.

Prézelin, B. B. 1992. Diel periodicity in phytoplankton productivity. Hydrobiologia **238**: 1-35.

Smith, R. C., and K. S. Baker. 1978. The bio-optical state of ocean waters and remote sensing. Limnol. Oceanogr. **23**: 247-259.

Sosik, H. M., and B. G. Mitchell. 1991. Absorption, fluorescence, and quantum yield for growth in nitrogen-limited *Dunaliella tertiolecta*. Limnol. Oceanogr. **36**: 910-921.

Sournia, A. 1974. Circadian periodicities in natural populations of marine phytoplankton. Adv. Mar. Biol. **12**: 325-389.

Stramski, D., and A. Morel. 1990. Optical properties of photosynthetic picoplankton in different physiological states as affected by growth irradiance. Deep-Sea Res. **37**: 245-266.

Stramski, D., A. Morel, and A. Bricaud. 1988. Modeling the light attenuation and scattering by spherical phytoplanktonic cells: a retrieval of the bulk refractive index. Applied Optics **27**: 3954-3957.

Stramski, D., and R. A. Reynolds. 1993. Diel variations in the optical properties of a marine diatom. Limnol. Oceanogr. **38**: 1347-1364.

Stramski, D., A. Shalapyonok, and R. A. Reynolds. 1995. Optical characterization of the oceanic unicellular cyanobacterium *Synechococcus* grown under a day-night cycle in natural irradiance. J. Geophys. Res. **100**: 13295-13307.

Thompson, P. A., P. J. Harrison, and J. S. Parslow. 1991. Influence of irradiance on cell volume and carbon quota for ten species of marine phytoplankton. J. Phycol. **27**: 351-360.

van de Hulst, H. C. 1957. Light scattering by small particles. Wiley.

Werner, D. 1977. The biology of diatoms. Univ. California Press.

Notation

λ	Light wavelength *in vacuo*, nm
a, b, c	Absorption, scattering, and attenuation coefficients of suspension, m^{-1}
σ_a , σ_b , σ_c	Absorption, scattering, and attenuation cross-sections, m^2 $cell^{-1}$
Q_a , Q_b , Q_c	Absorption, scattering, and attenuation efficiency factors, dimensionless
m	Complex index of refraction relative to seawater, dimensionless
n	Real part of the complex index of refraction, dimensionless
n'	Imaginary part of the complex index of refraction, dimensionless
n_w	Refractive index of seawater, dimensionless
D, G, V	Cell diameter (μm), projected-area (μm^2), and volume (μm^3)
F(D)	Density function of size distribution, cells m^{-3} μm^{-1}
Chl a_i	Intracellular concentration of chlorophyll *a*, kg m^{-3}
Car_i	Intracellular concentration of carotenoid pigments, kg m^{-3}
C_i	Intracellular concentration of carbon, kg m^{-3}
a^*_{Chl}	Chlorophyll *a*-specific absorption coefficient, m^2 (mg chlorophyll *a*)$^{-1}$
b^*_{Chl}	Chlorophyll *a*-specific scattering coefficient, m^2 (mg chlorophyll *a*)$^{-1}$

In the text, a bar is used over a symbol to indicate the quantity represents a mean value calculated from the polydispersed population of cells.

Table 1. Mean cell volume, elemental composition, and pigmentation for *Thalassiosira pseudonana* cells grown in nitrate-limited semicontinuous culture at 20°C. A growth irradiance of 345 μmol m^{-2} s^{-1} (scalar photosynthetically available radiation) was provided over a 12 h photoperiod. Nitrogen-specific net growth rates (μ_N) were calculated from the rate of dilution with fresh media, and are statistically insignificant from measured growth rates. For each growth rate, results are presented for two experiments in which sampling was performed at either the dark-to-light transition (D-L) or at the light-to-dark transition (L-D). Carbon and pigment data are given as concentrations per cell volume. The data represent the mean of 3 to 4 consecutive days of measurements at steady state, with the coefficient of variation (in percent) within parentheses.

μ_N [d^{-1}]	Time of sampling	$\bar{V}$ [μm^3]	C_i [kg m^{-3}]	C:N atomic ratio	Chl a_i [kg m^{-3}]	Car_i [kg m^{-3}]
0.22	D-L	54 (0.7)	171 (3.1)	17.4 (1.2)	1.2 (2.6)	0.92 (1.2)
	L-D	62 (3.1)	192 (0.4)	18.1 (1.2)	1.1 (1.0)	0.91 (2.5)
0.51	D-L	56 (0.7)	132 (2.3)	15.9 (2.4)	1.4 (2.0)	0.88 (1.0)
	L-D	69 (1.7)	185 (3.7)	20.7 (1.3)	1.5 (4.0)	0.98 (3.5)
0.81	D-L	56 (1.3)	121 (1.9)	13.0 (0.4)	1.9 (3.3)	1.07 (3.6)
	L-D	62 (2.9)	193 (3.4)	19.4 (1.2)	2.2 (4.7)	1.36 (4.8)
1.32	D-L	72 (1.9)	95 (5.5)	5.5 (5.9)	3.4 (4.8)	1.38 (5.2)
	L-D	71 (3.1)	186 (2.5)	14.8 (2.8)	3.3 (2.3)	1.75 (3.6)

Figure Legends

Fig. 1. Density function of size distribution for *Thalassiosira pseudonana* cells measured at four nitrogen-limited growth rates. Each distribution has been normalized to the total number of cells for ease of comparison, and represents the average of 3 to 4 consecutive days of measurements at steady state. A. Experiments in which sampling of the culture was done at the D-L transition. B. Experiments in which sampling was done at the L-D transition.

Fig. 2. The bulk refractive index of *T. pseudonana* cells at four nitrogen-limited growth rates. Filled symbols represent D-L transition experiments, open symbols represent L-D transition experiments. Each data point represents the average of 3 to 4 consecutive days of sampling at steady state. Error bars depict 1 SD of the mean and are omitted when smaller than the symbolic representation of the data point. A. Imaginary part of refractive index at indicated light wavelengths. B. Real part of refractive index at 660 nm.

Fig. 3. Mean cell absorption cross-sections for nitrogen-limited *T. pseudonana.* A. Spectral absorption cross-sections at indicated growth rates. The bold lines represent D-L transition experiments, whereas the light lines represent L-D transition experiments. Each spectra represents the average of 3 to 4 days of measurements at steady state. B. Absorption cross-sections at indicated light wavelengths as a function of nitrogen-specific growth rate. Symbols as in Fig. 2.

Fig. 4. As in Fig. 3, but for scattering cross-sections.

Fig. 5. Scattering-to-absorption ratios, at indicated light wavelengths, as a function of nitrogen-specific growth rate in *T. pseudonana.* Symbols as in Fig. 2.

Fig. 6. Chlorophyll *a*-specific optical coefficients as a function of nitrogen-specific growth rate for cultures of *T. pseudonana*. Symbols as in Fig. 2. A. Chl a-specific absorption at indicated light wavelengths. B. Chl a-specific scattering at 660 nm.

Fig. 7. The real and imaginary components of the refractive index as a function of biochemical composition for *T. pseudonana*. The data points represent the combined data from all experiments, with each point depicting an individual day of sampling. The regression line in each panel represents the least squares best-fit to the data (Model I regression), the regression formula and squared correlation coefficient are included in each panel. A. The imaginary part of the refractive index (at 673 nm) as a function of intracellular Chl a concentration. B. The real part of the refractive index (at 660 nm) as a function of intracellular carbon concentration.

Fig. 8. The relationship between Chl a-specific absorption (at indicated light wavelengths) and the product Chl a_i $\overline{D}$, where Chl a_i is the intracellular concentration of Chl a and $\overline{D}$ is the mean cell diameter.

Fig. 9. The Chl a-specific scattering coefficient (at 660 nm) as a function of the cellular carbon to chlorophyll *a* ratio. Data points and results of the regression analysis are included as in Fig. 7.

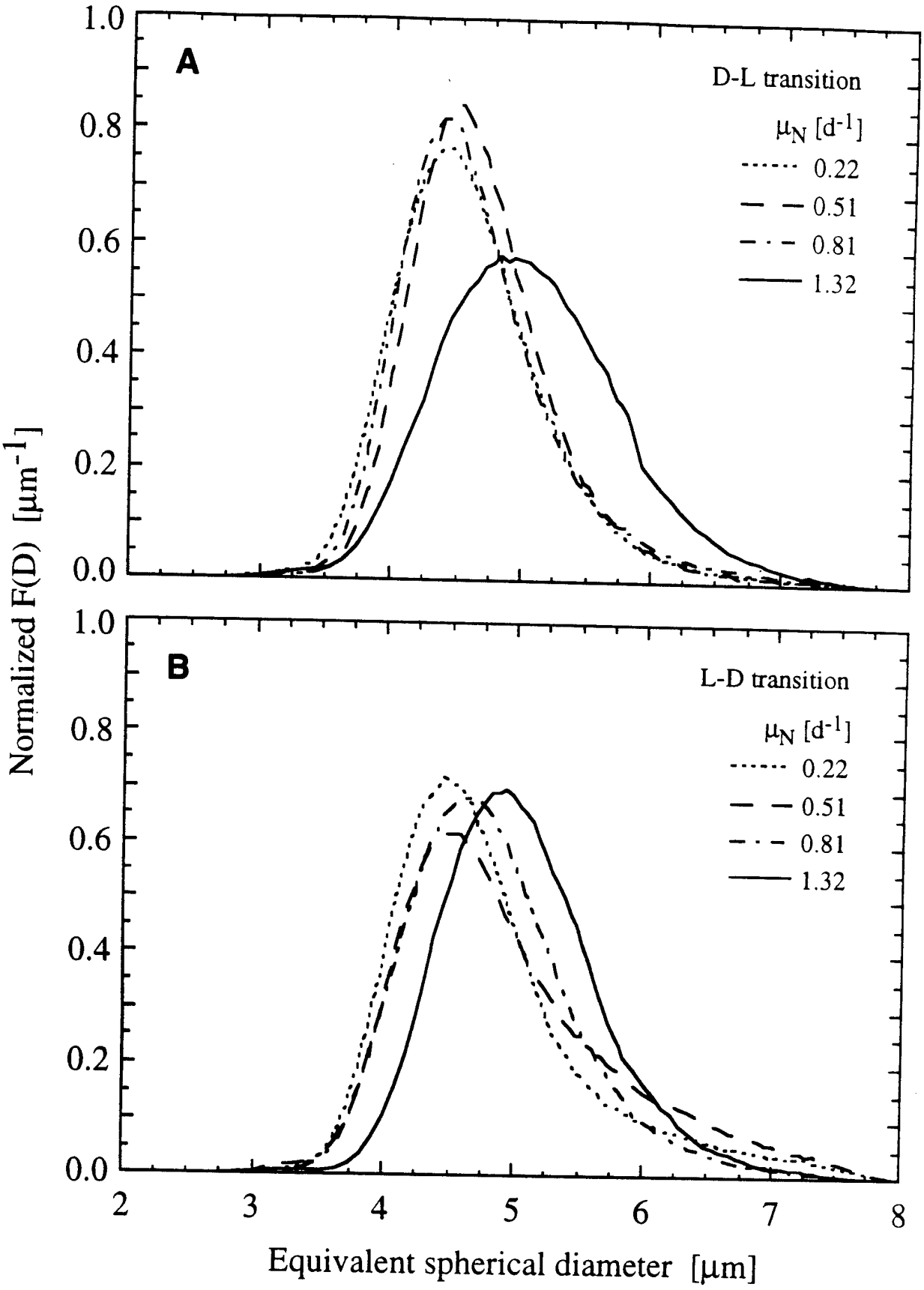
A
D-L transition
μ_N [d^{-1}]
0.22
0.51
0.81
1.32
B
L-D transition
μ_N [d^{-1}]
0.22
0.51
0.81
1.32
Normalized F(D) [µm^{-1}]
Equivalent spherical diameter [µm]
0.0
0.2
0.4
0.6
0.8
1.0
2
3
4
5
6
7
8

Fig. 1

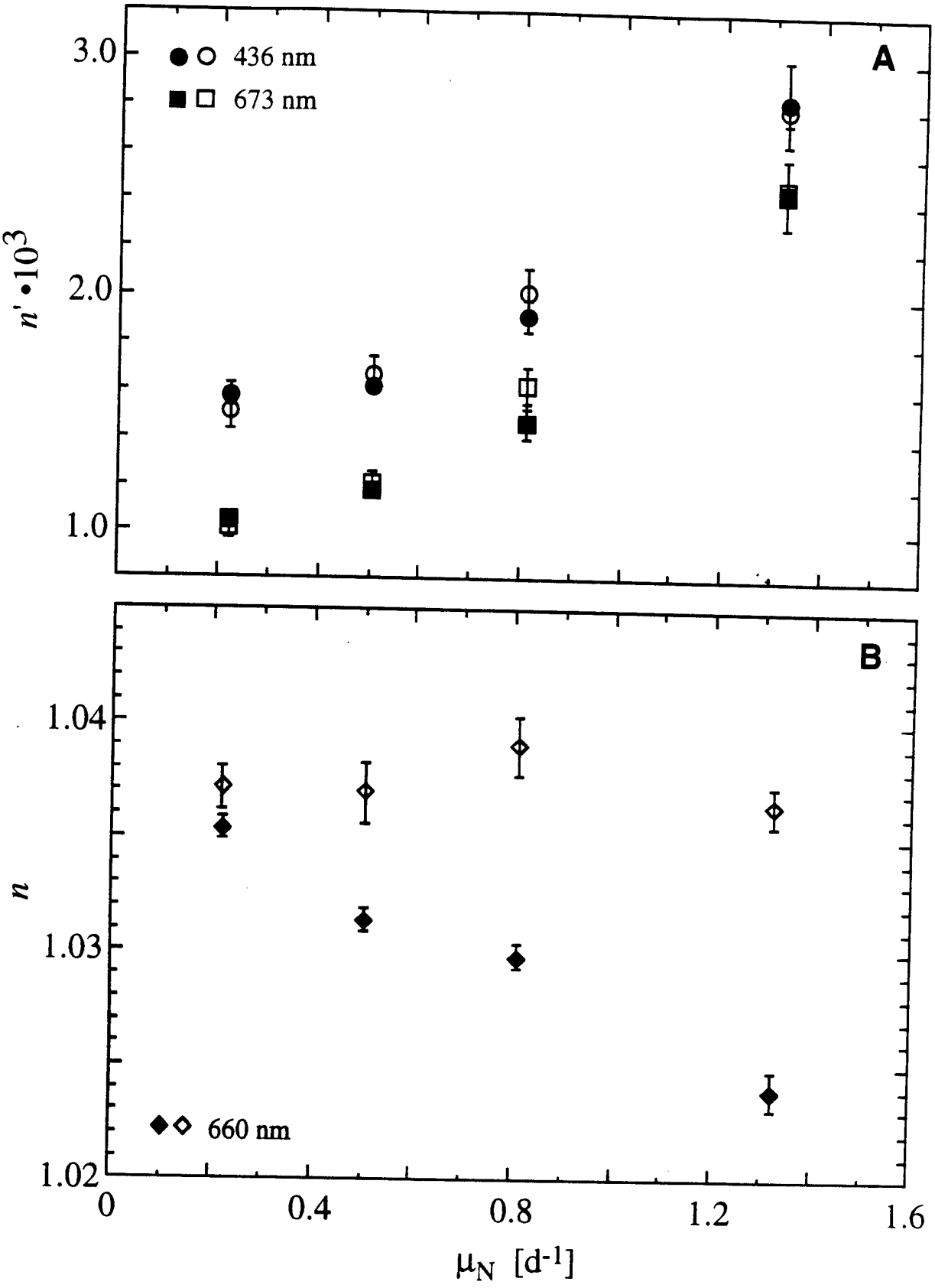
A
B
436 nm
673 nm
660 nm
n' •10^3
n
μN [d-1]
3.0
2.0
1.0
1.04
1.03
1.02
0
0.4
0.8
1.2
1.6

Fig. 2

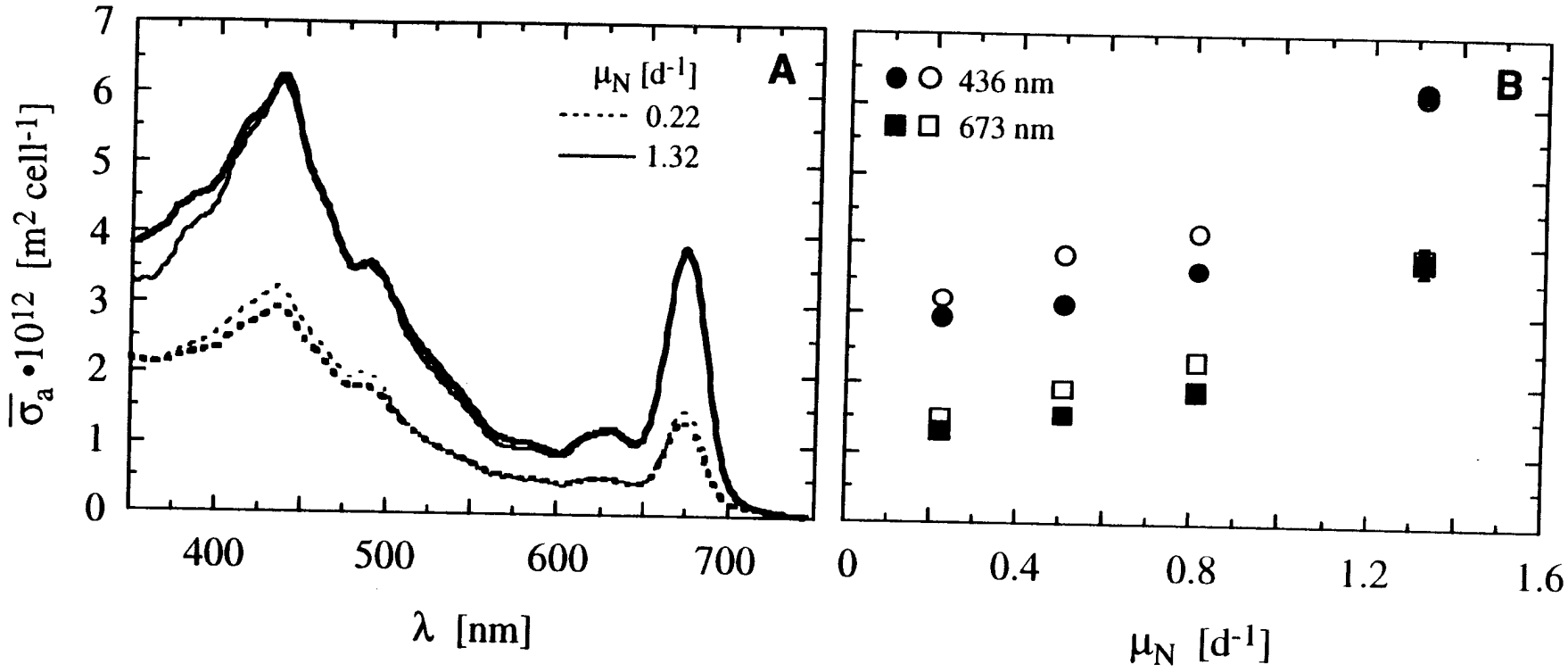
A
μ_N [d^{-1}]
0.22
1.32
$\overline{\sigma}_a \cdot 10^{12}$ [m^2 cell^{-1}]
λ [nm]
B
436 nm
673 nm
μ_N [d^{-1}]

Fig. 3

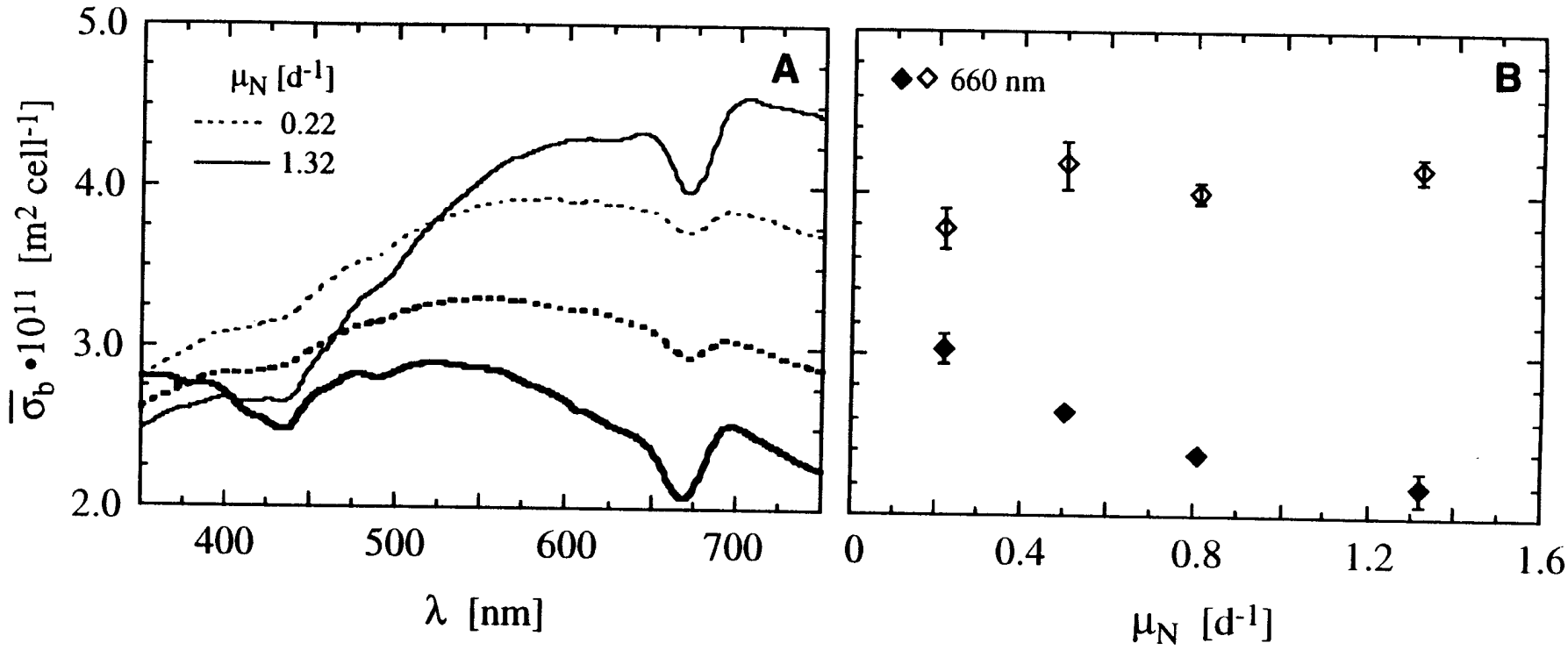
5.0
4.0
3.0
2.0
$\overline{\sigma}_b \cdot 10^{11}$ [m^2 cell^{-1}]
μ_N [d^{-1}]
0.22
1.32
A
400
500
600
700
λ [nm]
660 nm
B
0
0.4
0.8
1.2
1.6
μ_N [d^{-1}]

Fig. 4

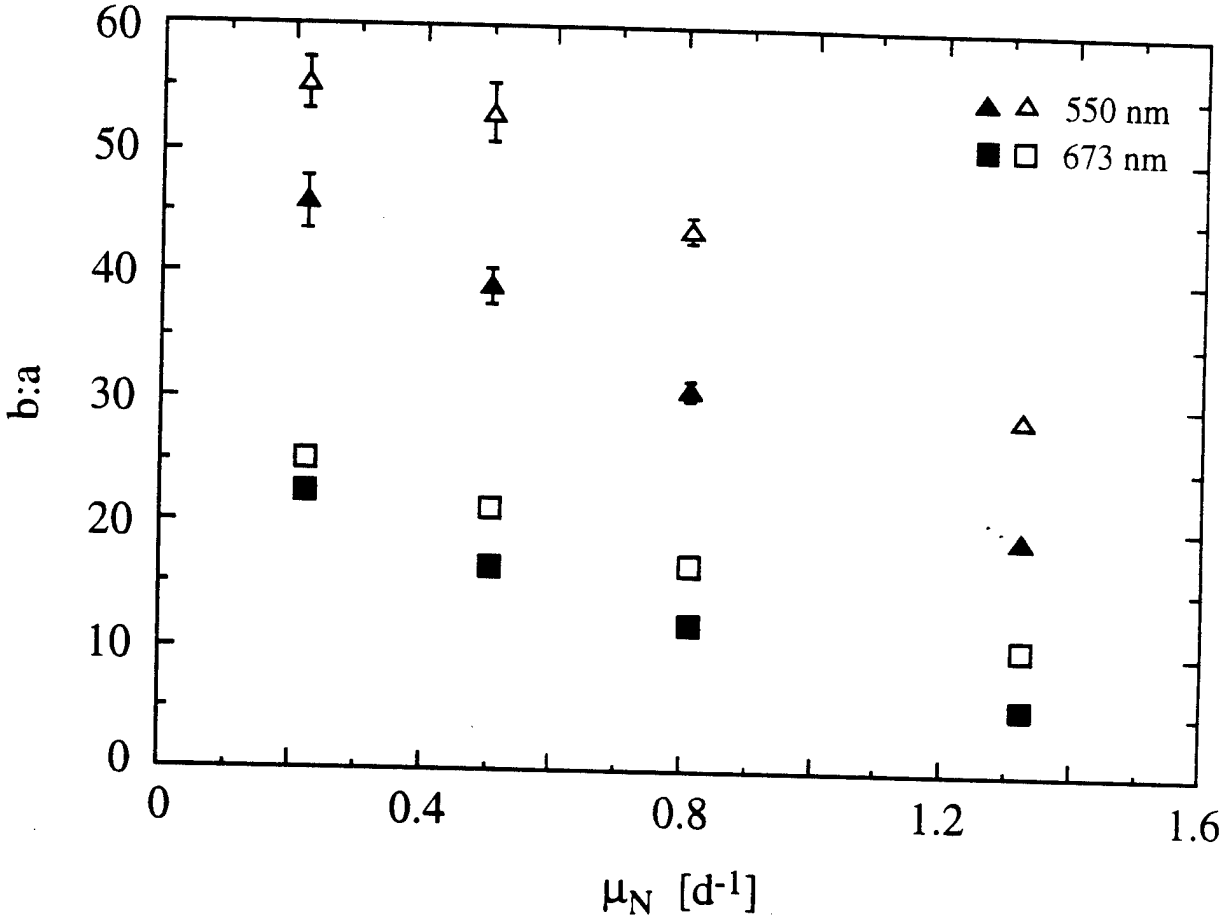

Fig. 5

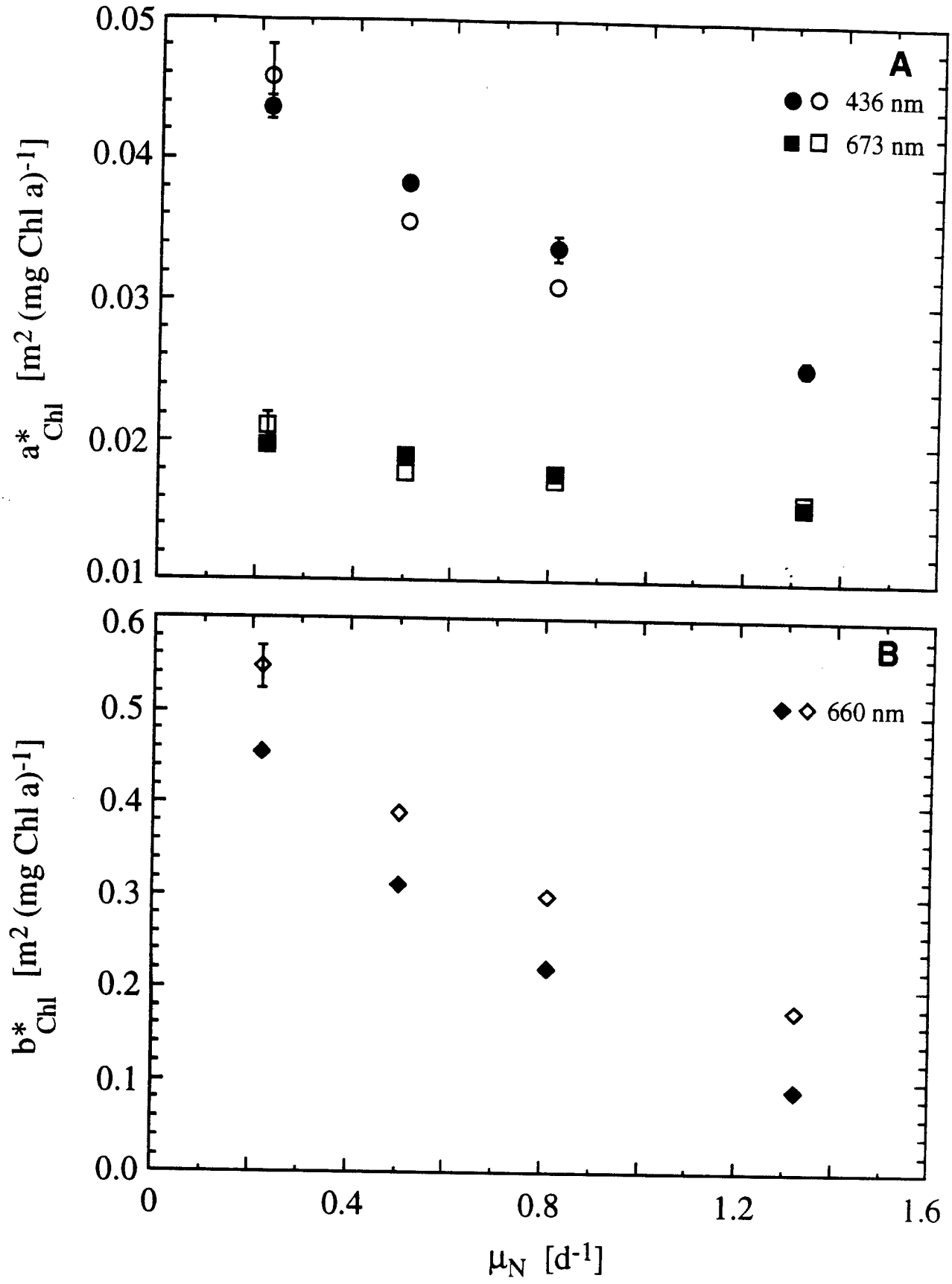
A
436 nm
673 nm
a^*_{Chl} [m^2 (mg Chl a)$^{-1}$]
0.05
0.04
0.03
0.02
0.01
B
660 nm
b^*_{Chl} [m^2 (mg Chl a)$^{-1}$]
0.6
0.5
0.4
0.3
0.2
0.1
0.0
0
0.4
0.8
1.2
1.6
μ_N [d^{-1}]

Fig. 6

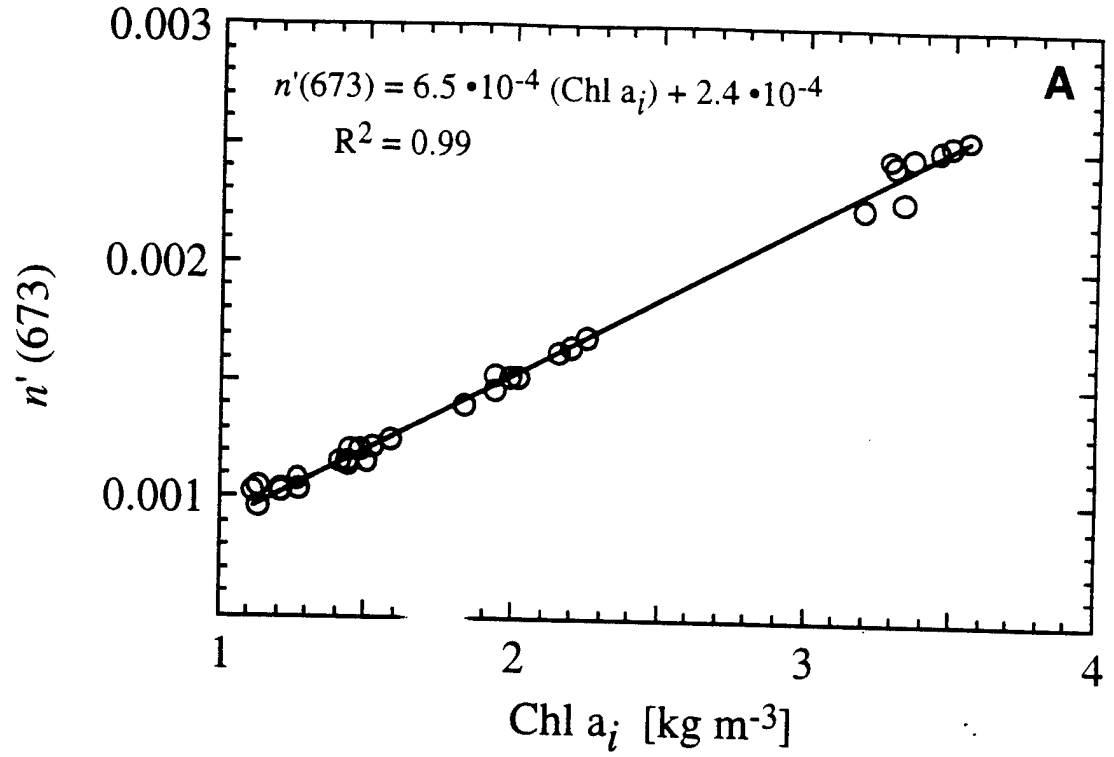
0.003
0.002
0.001
n' (673)
n'(673) = 6.5 •10-4 (Chl ai) + 2.4 •10-4
R2 = 0.99
A
1
2
3
4
Chl ai [kg m-3]

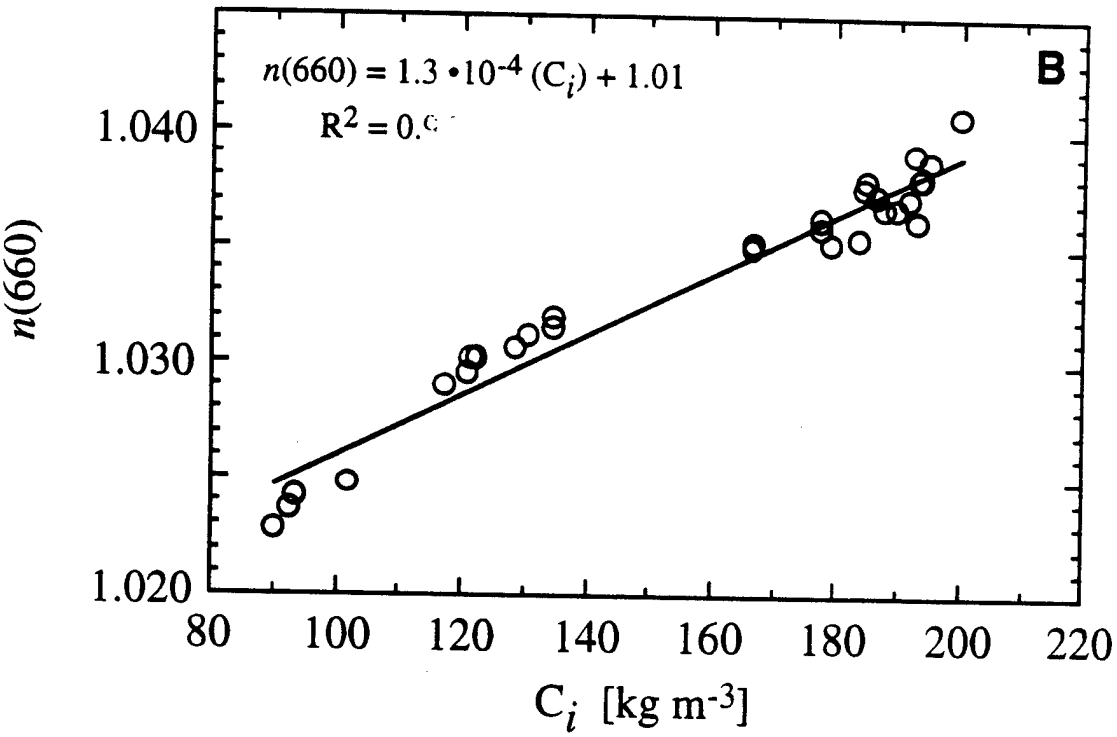
n(660) = 1.3 •10-4 (Ci) + 1.01
B
1.040
1.030
1.020
n(660)
80
100
120
140
160
180
200
220
Ci [kg m-3]

Fig. 7

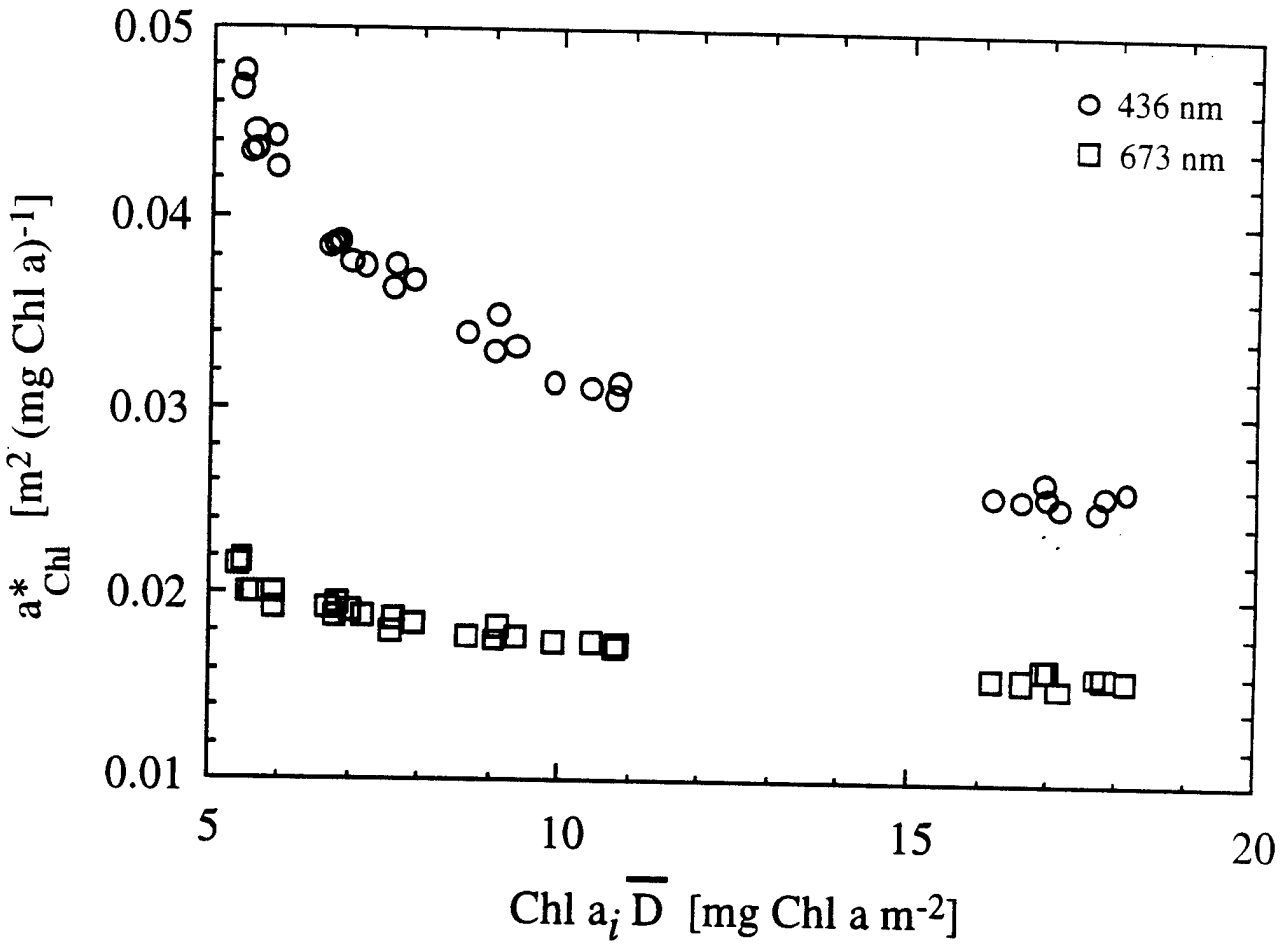
0.05
0.04
0.03
0.02
0.01
5
10
15
20
436 nm
673 nm
a^*_{Chl} [m^2 (mg Chl a)$^{-1}$]
Chl a_i $\overline{D}$ [mg Chl a m^{-2}]

Fig. 8

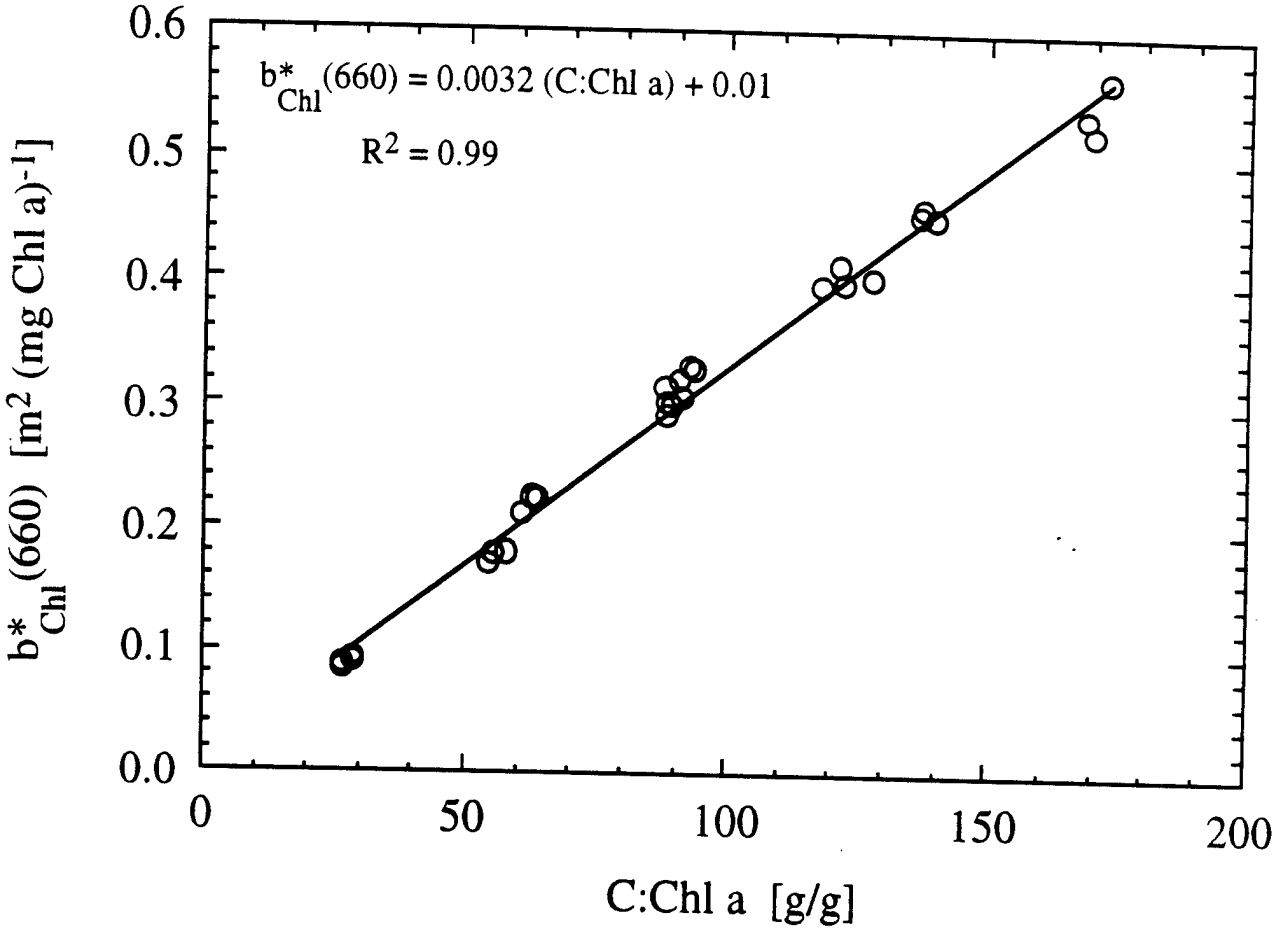
$b^*_{Chl}(660) = 0.0032$ (C:Chl a) + 0.01
$R^2 = 0.99$
$b^*_{Chl}(660)$ [m^2 (mg Chl a)$^{-1}$]
C:Chl a [g/g]
0.0
0.1
0.2
0.3
0.4
0.5
0.6
0
50
100
150
200

Fig. 9